

High-Pressure Synthesis and Characterization of Incompressible Titanium Pernitride

Venkata S. Bhadram,* Duck Young Kim, and Timothy A. Strobel*

HPSTAR
2016-193

Geophysical Laboratory, Carnegie Institution of Washington, Washington, DC 20015, United States

S Supporting Information

Transition metal nitrides represent an important class of materials exhibiting a wide variety of properties including high refractivity,¹ superconductivity,² and recently, electrocatalytic activity.^{3,4} Most transition metal nitrides exist with ratios of N:M \leq 1 (M-metal) and they exhibit metallic properties. On the other hand, nitrogen-rich transition metal pernitrides, which can be synthesized at high pressures, exhibit superior properties as compared to the corresponding nitrides.^{5–9}

In the recent past, there has been enormous attention to transition metal pernitrides after the successful synthesis of ultraincompressible PtN₂ with a bulk modulus 372 GPa.⁵ The search for the other transition metal pernitrides led to the discovery of OsN₂,¹⁰ IrN₂,^{5,10,11} PdN₂,¹¹ RuN₂,¹² and RhN₂.¹³ The structures of these materials contain pernitride (N₂⁴⁻) units that are encapsulated in the metal lattice and are isoelectronic to peroxide ions (O₂²⁻, also isoelectronic with molecular fluorine), hence the name pernitride. They exhibit three main types of crystal structures: PtN₂ and PdN₂ crystallize in the pyrite (cubic *Pa* $\bar{3}$) structure;^{5,11} IrN₂ exhibits the arsenopyrite-type structure, while OsN₂, RhN₂, and RuN₂ crystallize in the marcasite (orthorhombic *Pnmm*)^{14–16} structure. Although their space groups are different, most pernitrides can be characterized by nitrogen atoms octahedrally coordinating metal atoms to form MN₆ octahedra that are interconnected in three dimensions through dinitrogen (N–N) bonds. Here, the covalent N–N interactions are of single bond in nature, as indicated by strong first-order Raman modes near 1000 cm⁻¹ (compare with hydrazine N₂H₄), as observed for nonmetallic samples.^{5,10,17} The N–N bond length in PtN₂ and OsN₂ is between 1.4 and 1.42 Å, which is close to the bond length of ultraincompressible, single-bonded polymeric nitrogen.¹⁷ Previous studies suggest that the extraordinary mechanical and electronic properties of transition metal pernitrides may originate from metal–nitrogen charge transfer and the nature of the N–N bonds.^{18–20} Thus, synthesis of new pernitrides and an understanding their bonding character is not only important from a fundamental perspective but also essential for realizing new materials with technological applications.

In this communication, we discuss the synthesis and characterization of titanium pernitride (TiN₂). This new nitride is incompressible with a bulk modulus in the range of 360–385 GPa and is expected to be the hardest among all Ti–N compounds.²¹ We have used *ab initio* calculations based on density functional theory (DFT)^{22,23} to understand the crystal structure, thermodynamic properties, and bonding nature of TiN₂. Although there were a few theoretical reports that

predicted the crystal structure and properties of TiN₂ before,^{21,24} there was no prior experimental evidence to validate these predictions. Previous attempts of the synthesis of nitrogen-rich titanium nitrides was unsuccessful, possibly due to the choice of the starting materials and synthesis conditions.²⁵

TiN₂ was synthesized using the laser-heated diamond anvil cell technique at 73(3) GPa and 2400(40) K. The starting materials consisted of a small (10 × 15 × 5 μm³) flake of TiN loaded in the DAC that was surrounded by a dense N₂ pressure transmitting medium. After compression, samples were heated using an infrared laser and then probed by X-ray diffraction (XRD) (see methods in Supporting Information). The X-ray diffraction pattern of the laser heated sample (Figure 1a) is dominated by Bragg peaks from solid molecular nitrogen that surrounded the original TiN sample on all sides and represented the majority of the sample chamber volume. Some of these peaks are consistent with the reported structure of ζ-N₂,^{26,27} however, the exact structure of N₂ at these thermodynamic conditions is currently unresolved. Nevertheless, the N₂ Bragg reflections are unambiguously identified by probing the sample volume containing only pure N₂. In addition to these reflections, we also observed new sharp and well-resolved peaks in the pattern that can be easily indexed to a tetragonal unit cell (space group *I4/mcm*) with lattice parameters of *a* = *b* = 4.092(1) Å and *c* = 4.974(1) Å at 73 GPa. These parameters are in excellent agreement with recent predictions of Yu et al.²¹ for the CuAl₂-type TiN₂ structure and indicate the formation of this phase. This is in contrast to Kulkarni et al.²⁴ who suggested the possibility for TiN₂ with the orthorhombic *Pmn*2₁ type structure.

On decompression, we found that this phase is recoverable to ambient conditions and remains mechanically stable in air. The phase determination of the recovered sample confirms the high pressure indexing and removes any uncertainties associated with overlapping ζ-N₂ peaks as all gaseous N₂ was evacuated from the cell at 0 GPa. The TiN₂ phase remains in the tetragonal *I4/mcm* structure at ambient conditions with lattice parameters *a* = *b* = 4.334(1) Å and *c* = 5.294(2) Å. Apart from TiN₂ and some unreacted TiN, we also observed diffraction lines from rhenium as the sample moved close to the gasket edge during decompression. Based on two-dimensional diffraction images (as shown in Figure S2), which show “spotty” Debye–Scherrer rings with strong

Received: January 5, 2016

Revised: February 29, 2016

Published: March 7, 2016

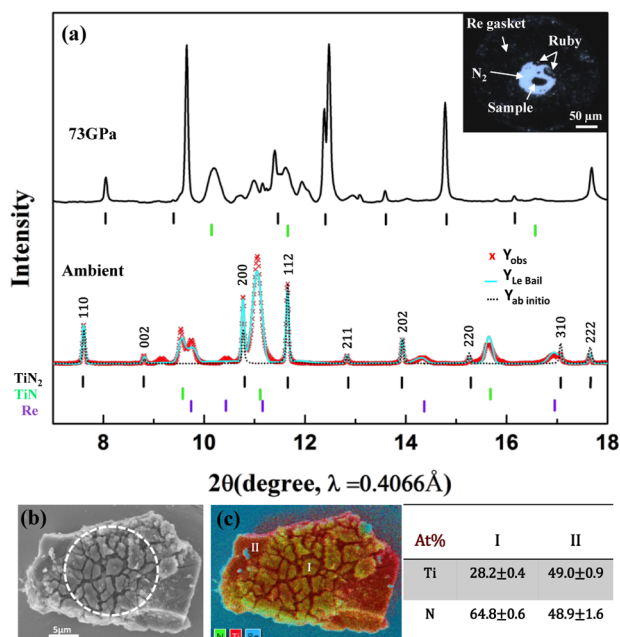


Figure 1. (a) X-ray diffraction patterns of laser heated TiN + N₂ system. The black tick marks indicate the Miller indices of the tetragonal *I4/mcm* lattice. Optical micrograph shows the rhenium gasket and sample at 73 GPa inside the diamond anvil cell. (b) Scanning electron microscopy image of the recovered sample. The laser heated spot is encircled. (c) The energy dispersive X-ray spectroscopy map of the recovered sample where the colors indicate relative concentrations of the various elements. The concentration of Ti and N at two different spots in the heated and unheated regions on the sample is listed in the table.

azimuthal variations in intensity, the as-synthesized TiN₂ phase is of polycrystalline nature with individual grains of comparable size to the synchrotron beam (i.e., ~5 μm). It was therefore not possible to perform quantitative Rietveld refinements on integrated one-dimensional patterns to precisely determine atomic positions. Nevertheless, the integrated intensities of all observed reflections qualitatively correspond with predicted intensities (see Figure 1a) derived from the ab initio *I4/mcm* structural model using nitrogen atoms at 8h Wyckoff positions ($x = 0.1124$). Thus, the synthesis of *I4/mcm* TiN₂ is confirmed through this qualitative intensity agreement and excellent quantitative agreement in unit cell symmetry and lattice parameters.

Scanning electron microscopy images obtained from the recovered sample (as shown in Figure 1b) show cracks leading to texturing of the laser heated area, which indicates recrystallization due to chemical reaction of TiN with N₂. The large volume difference between TiN and TiN₂ likely facilitates this cracking and texturing of the laser heated area. Energy dispersive spectroscopic (EDS) analysis of the recovered sample is shown in Figure 1c. The EDS layered image shows strong contrast between the heated and unheated areas, demonstrating the presence of a higher concentration of nitrogen in this region as compared to the rest of the sample. The estimated atomic ratio between Ti and N in the heated region gives stoichiometries varying between 1:2 and 1:2.5, whereas the nonheated area gives a ratio of 1:1. The variation in stoichiometry of the sample in the heated region could be due to the orientations of TiN₂ grains which yield topography-related errors in EDS analysis. Nevertheless, the measured

compositions in the heated and nonheated regions provide further confirmation for the formation of TiN₂.

Further insights into the new phase can be gained by comparing its volume versus pressure data (P - V data) with that of the reactants (i.e., TiN + 1/2N₂). The necessary thermodynamic condition for the pressure-induced chemical reaction is that the volume per atom of the products must be smaller than that of the reactant phases throughout the pressure range. It is evident from Figure 2 that the measured volume per

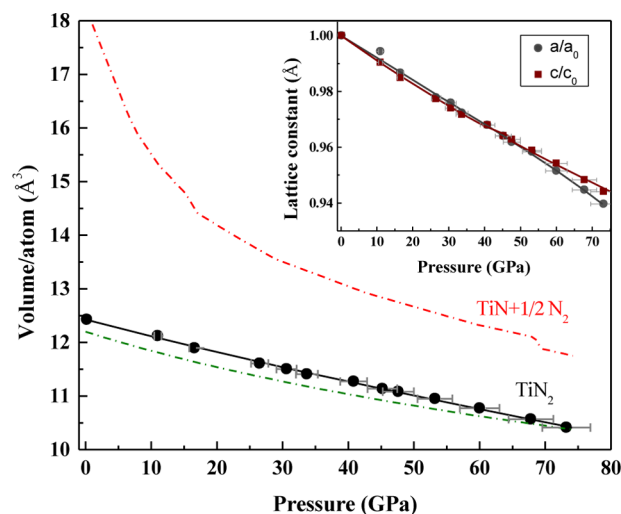


Figure 2. Experimental pressure–volume data of TiN₂ (black circles) compared with the pressure–volume relation of the reactants, i.e., TiN + 1/2N₂ (pink dotted line) at room temperature. Inset shows the pressure dependence of the lattice parameters a and c (solid symbols). The solid lines are the EoS fit to the experimental data. The green dotted line is the calculated EoS of TiN₂ using PBESol for the *I4/mcm* structure ($V_0 = 97.61 \text{ \AA}^3$, $K_0 = 328 \text{ GPa}$, $K'_0 = 4.0$). The error values for the lattice parameters are smaller than the size of the symbols.

atom of TiN₂ is always smaller than that of TiN + 1/2N₂. The huge volume difference (~11%) between the reactants and the product indicates that the reaction product is indeed a new compound (as opposed to a phase transition in TiN).

The P - V data were fitted using the third order Birch–Murnaghan equation of state (EoS) (as shown in Figure 2). The zero-pressure bulk modulus, $K_0 = 385(7)$ (with $K'_0 = 1.45(18)$) obtained here is far higher than all other known phases in the Ti–N system.²¹ Also, the measured bulk modulus is close to that of c-BN ($K_0 = 382(3)$, $K'_0 = 4.46(15)$)²⁸ indicating that tetragonal TiN₂ is incompressible and could be a potential superhard material (a thermodynamic model suggests a hardness near 30 GPa²¹). It is to be noted that the refined value for K'_0 is lower than that obtained for most materials. It is quite normal that the parameters K_0 and K'_0 correlate heavily while fitting the compression data using EoS fit.²⁹ This means the data can be fitted almost equally well by decreasing the value of K_0 and increasing the value of K'_0 or vice versa. To better illustrate the extent of correlation between K_0 and K'_0 and to see the range of possible values for K_0 and K'_0 , we have used 3 σ , 2 σ , and 1 σ confidence ellipses in the parameter space of K_0 and K'_0 as shown in the Supporting Information (see Figure S3a). The K'_0 value is less than 2 even at 99.73% confidence level. Correspondingly, K_0 acquires values higher than 360 GPa. Looking at these confidence ellipses, we can unequivocally report that the bulk modulus of TiN₂ is higher than 360 GPa.

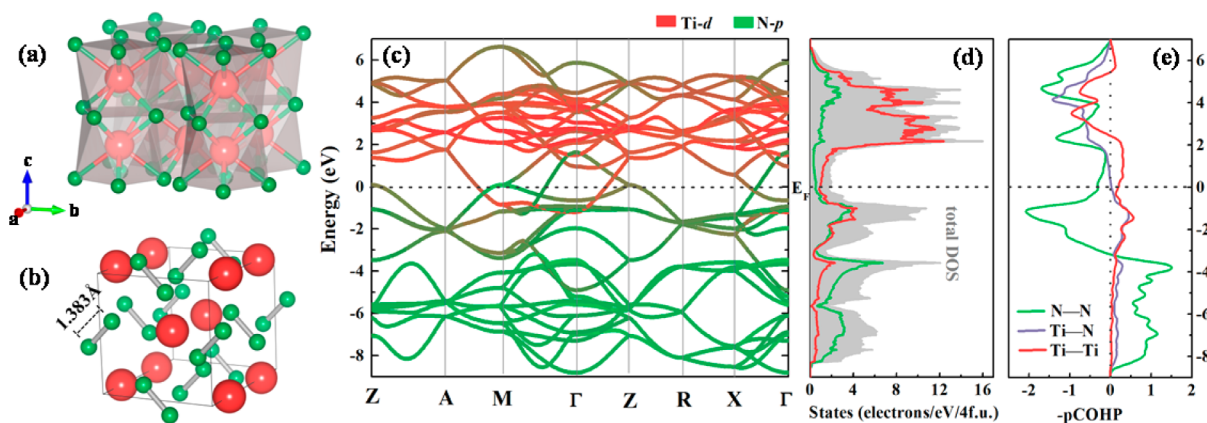


Figure 3. (a, b) crystal structure of $I4/mcm$ TiN_2 with N–N dumbbells; (c) fat-band plot of TiN_2 with Ti- d and N- p characteristics. The notation of the symmetry points is as follows: Z (0, 0, 1/2); A (1/2, 1/2, 1/2); M (1/2, 1/2, 0); Γ (0, 0, 0); Z (0, 0, 1/2); R (0, 1/2, 1/2); X (0, 1/2, 0); and Γ (0, 0, 0). (d) Total and partial density of states (DOS). (e) Projected Crystal Orbital Hamilton Population ($-pCOHP$) analysis of various bonds in TiN_2 . The Fermi level (E_F) is indicated by gray dashed line.

The thermodynamic behavior of TiN_2 was investigated further via ab initio (DFT) calculations using different functionals (PBE,^{30,31} PBEsol,³² and LDA). The formation enthalpy of TiN_2 at 1 atm is 0.386 eV/atom, and it is also metastable with respect to disproportionation into $TiN + N_2$. The calculated structural and EoS parameters are summarized in Table S1. The calculated bulk moduli are systematically lower than the estimated value from experiment, which was also observed for several other pernitride systems.^{10,19,33} The discrepancy here is the consequence of a monotonically increasing under-prediction of the experimental lattice parameters as pressure decreases from 73 GPa. Nevertheless, PBEsol showed the best agreement with experiment (Figure 2) with an average deviation of only -1.7% over the entire pressure range.

The structure of TiN_2 is $CuAl_2$ -type with 4 formula units per unit cell. It consists of layers of N_2 and Ti stacked along the c -axis. Unlike other metal pernitrides, which usually contain MN_6 (M-metal) octahedra, TiN_2 contains TiN_8 face-sharing tetragonal antiprisms stacked along the c -axis (as shown in Figure 3a). The neighboring antiprisms along the a and b -axes are connected through N_2 -dumbbells (see Figure 3b) and is analogous to the structure of SrS_2 .³⁴ The separation between two neighboring N_2 -dumbbells along the a -axis is larger than that along the c -axis, and the dihedral angles between two neighboring N_2 -dumbbells along c - and a -axes are 86.3° and 180.0° , respectively. This observation suggests that the nearest-neighbor N_2 dumbbells along the c -axis are oriented with respect to each other to minimize steric hindrance. Based on our ab initio calculations, the N–N bond distance at ambient pressure is found to be 1.383 Å and is comparable to the F–F bond length (1.42 Å) in molecular F_2 and the N–N bond length in pernitrides of some transition metals such as PtN_2 (1.41 Å) and OsN_2 (1.43 Å).^{5,10} This distance indicates that the N_2 dumbbells in TiN_2 exist as N_2^{4-} (pernitride ions with N–N single bonds). This is in contrast with N_2^{2-} ions, observed for example in BaN_2 , which exhibits $N=N$ bond lengths of 1.23 Å.²⁰ Further confirmation for N–N bonding character can be gained from the vibrational frequency of the dinitrogen units. Unfortunately, the Raman spectrum of TiN_2 collected using a low laser power shows no Raman signal (see Figure S4) likely due to the metallic nature of this phase, as predicted previously²¹ and consistent with the absence of Raman signal in other metallic pernitrides.^{10,12} However, the theoretically

predicted N–N vibrational frequency is $\sim 1150\text{ cm}^{-1}$ which is higher than that of PtN_2 (860 cm^{-1})⁵ and much lower than that of BaN_2 (1466 cm^{-1}).²⁰ This confirms that the N–N bonds within TiN_2 are of single bond character and the bonding is slightly stronger as compared with PtN_2 as reflected in both bond length and vibrational frequency.

To gain deeper insights into the electronic properties and bonding features of TiN_2 , we have performed electronic band structure calculations based on DFT using PBEsol. The orbital-resolved “fat-band” plot for TiN_2 at ambient pressure along high-symmetry directions is shown in Figure 3c. It is clear from this electronic band structure that TiN_2 is metallic and several bands are crossing the Fermi level (E_F), which is set to zero in the plot. The fat-bands show different atomic orbital contributions to the conduction bands and are comprised of mixed Ti- d and N- p states. Delocalized electrons at the top of the conduction bands that are responsible for metallicity originate from both Ti- d and Ti- d /N- p hybrid electrons. The complete picture of chemical bonding within TiN_2 is complex and clearly of mixed character. While formally metallic, the DOS at the Fermi energy is low (1.8 states/eV/4f.u.) and a broad pseudogap is formed between occupied hybrid Ti- d /N- p states (below E_F) and unoccupied states (above E_F) with predominately Ti- d character. These features have been used as indicators of covalency in related materials.^{33,35} Covalent character between Ti and N is also indicated by the concurrence between bonding orbital character in Ti–N $-pCOHP$ (projected Crystal Orbital Hamilton Population^{36–38}) analysis and by the presence of hybrid Ti- d /N- p electrons between -8.5 eV up to E_F in the partial DOS. As indicated by Yu et al.²¹ and verified here by $-pCOHP$ analysis, the antibonding $1\pi_g^*$ orbitals (starting near -2 eV) are almost completely occupied at the top of the conduction band, and a portion of the metallic nature can be ascribed to these states being occupied at the Fermi level. As suggested by Wessel et al.²⁰ for the case of PtN_2 , charge transferred from Pt to N results in the filling of antibonding $1\pi_g^*$ states of N_2^{4-} . This filling serves to elongate the N–N bonds and, in conjunction with Coulomb repulsion,¹⁹ makes the system more resistant to external stress and results in high mechanical strength of the system. While there are differences in electronic and structural configurations, this mechanism is also at play for the case of TiN_2 although antibonding states are not completely filled and

N–N bonds are somewhat shorter. Bader charge analysis³⁹ indicates that 1.8 e⁻ are transferred from Ti to N₂, in contrast to 1.05 e⁻ for PtN₂ in the pyrite structure.⁴⁰ Overall these results indicate that TiN₂ can be viewed as possessing more ionic/metallic character than PtN₂ (covalent/ionic), although their mutual incompressibilities share similar origins.

In summary, we have synthesized a new transition metal pernitride, TiN₂, with tetragonal *I4/mcm* symmetry that exhibits a high bulk modulus. Based on our ab initio calculations, we tried to understand the bonding character and thereby the origin of high bulk modulus of TiN₂. The results presented here have important implications in synthesis of new metal nitrides and the understanding their structure–property relationships. We hope that our findings will encourage further theoretical and experimental work.

■ ASSOCIATED CONTENT

Supporting Information

The Supporting Information is available free of charge on the ACS Publications website at DOI: 10.1021/acs.chemmater.6b00042.

Experimental methods, computational details, and additional figures/table (PDF)

■ AUTHOR INFORMATION

Corresponding Authors

*(T.A.S.) E-mail: tstrob@ciw.edu.

*(V.S.B.) E-mail: vbhadram@ciw.edu.

Author Contributions

V.S.B. and T.A.S. have performed the experiments and analyzed the data. D.Y.K. has performed the theoretical calculations. The manuscript was written with contributions from all authors.

Notes

The authors declare no competing financial interest.

■ ACKNOWLEDGMENTS

We thank J. Armstrong for assistance with EDS measurements and R.J. Angel for valuable discussions. We also thank R. Hrubiak and H. Gou for assistance with XRD measurements. This work was supported by Energy Frontier Research in Extreme Environments (EFREE) Center, an Energy Frontier Research Center funded by the US Department of Energy, Office of Science, under Award No. DE-SC0001057. Portions of this work were performed at HPCAT (Sector 16), Advanced Photon Source (APS), Argonne National Laboratory. HPCAT operations are supported by DOE-NNSA under Award No. DE-NA0001974 and DOE-BES under Award No. DE-FG02-99ER45775, with partial instrumentation funding by the National Science Foundation (NSF). This research used resources of the National Energy Research Scientific Computing Center, a DOE Office of Science User Facility supported by the Office of Science of the U.S. Department of Energy under Contract No. DE-AC02-05CH11231 and the Extreme Science and Engineering Discovery Environments (XSEDE), which is supported by National Science Foundation grant number ACI-1053575.

■ REFERENCES

- (1) Pierson, H. O. *Handbook of refractory carbides and nitrides*, 1st ed.; Noyes Publications: Westwood, 1996.
- (2) Chen, X.-J.; Struzhkin, V. V.; Wu, Z.; Somayazulu, M.; Qian, J.; Kung, S.; Christensen, A. N. r.; Zhao, Y.; Cohen, R. E.; Mao, H.-k.

Hemley, R. J. Hard superconducting nitrides. *Proc. Natl. Acad. Sci. U. S. A.* **2005**, *102*, 3198–3201.

(3) Chen, W.-F.; Muckerman, J. T.; Fujita, E. Recent developments in transition metal carbides and nitrides as hydrogen evolution electrocatalysts. *Chem. Commun.* **2013**, *49*, 8896–8909.

(4) Zhang, Q.; Gao, L. Ta₃N₅ Nanoparticles with Enhanced Photocatalytic Efficiency under Visible Light Irradiation. *Langmuir* **2004**, *20*, 9821–9827.

(5) Crowhurst, J. C.; Goncharov, A. F.; Sadigh, B.; Evans, C. L.; Morrall, P. G.; Ferreira, J. L.; Nelson, A. J. Synthesis and Characterization of the Nitrides of Platinum and Iridium. *Science* **2006**, *311*, 1275–1278.

(6) von Appen, J.; Lumey, M. – W.; Dronskowski, R. Mysterious platinum nitride. *Angew. Chem., Int. Ed.* **2006**, *45*, 4365–4368.

(7) Salamat, A.; Hector, A. L.; Kroll, P.; McMillan, P. F. Nitrogen-rich transition metal nitrides. *Coord. Chem. Rev.* **2013**, *257*, 2063–2072.

(8) Auffermann, G.; Prots, Y.; Kniep, R. SrN and SrN₂: Diazenides by Synthesis under High N₂-Pressure. *Angew. Chem., Int. Ed.* **2001**, *40*, 547–549.

(9) Vajenine, G. V.; Auffermann, G.; Prots, Y.; Schnelle, W.; Kremer, R. K.; Simon, A.; Kniep, R. Preparation, Crystal Structure, and Properties of Barium Pernitride, BaN₂. *Inorg. Chem.* **2001**, *40*, 4866–4870.

(10) Young, A. F.; Sanloup, C.; Gregoryanz, E.; Scandolo, S.; Hemley, R. J.; Mao, H.-k. Synthesis of Novel Transition Metal Nitrides IrN₂ and OsN₂. *Phys. Rev. Lett.* **2006**, *96*, 155501.

(11) Crowhurst, J. C.; Goncharov, A. F.; Sadigh, B.; Zaug, J. M.; Aberg, D.; Meng, Y.; Prakapenka, V. B. Synthesis and characterization of nitrides of iridium and palladium. *J. Mater. Res.* **2008**, *23*, 1–5.

(12) Niwa, K.; Suzuki, K.; Muto, S.; Tatsumi, K.; Soda, K.; Kikegawa, T.; Hasegawa, M. Discovery of the Last Remaining Binary Lanthanum-Group Pernitride RuN₂. *Chem. - Eur. J.* **2014**, *20*, 13885–13888.

(13) Niwa, K.; Dzivenko, D.; Suzuki, K.; Riedel, R.; Troyan, I.; Eremets, M.; Hasegawa, M. High Pressure Synthesis of Marcasite-Type Rhodium Pernitride. *Inorg. Chem.* **2014**, *53*, 697–699.

(14) Yu, R.; Zhan, Q.; De Jonghe, L. C. Crystal Structures of and Displacive Transitions in OsN₂, IrN₂, RuN₂, and RhN₂. *Angew. Chem., Int. Ed.* **2007**, *46*, 1136–1140.

(15) Chen, Z. W.; Guo, X. J.; Liu, Z. Y.; Ma, M. Z.; Jing, Q.; Li, G.; Zhang, X. Y.; Li, L. X.; Wang, Q.; Tian, Y. J.; Liu, R. P. Crystal structure and physical properties of OsN₂ and PtN₂ in the marcasite phase. *Phys. Rev. B: Condens. Matter Mater. Phys.* **2007**, *75*, 054103.

(16) Wu, Z.-j.; Zhao, E.-j.; Xiang, H.-p.; Hao, X.-f.; Liu, X.-j.; Meng, J. Crystal structures and elastic properties of superhard IrN₂ and IrN₃ from first principles. *Phys. Rev. B: Condens. Matter Mater. Phys.* **2007**, *76*, 054115.

(17) Eremets, M. I.; Gavriluk, A. G.; Trojan, I. A.; Dzivenko, D. A.; Boehler, R. Single-bonded cubic form of nitrogen. *Nat. Mater.* **2004**, *3*, 558–563.

(18) Young, A. F.; Montoya, J. A.; Sanloup, C.; Lazzeri, M.; Gregoryanz, E.; Scandolo, S. Interstitial dinitrogen makes PtN₂ an insulating hard solid. *Phys. Rev. B: Condens. Matter Mater. Phys.* **2006**, *73*, 153102.

(19) Liu, Z. T. Y.; Gall, D.; Khare, S. V. Electronic and bonding analysis of hardness in pyrite-type transition-metal pernitrides. *Phys. Rev. B: Condens. Matter Mater. Phys.* **2014**, *90*, 134102.

(20) Wessel, M.; Dronskowski, R. Nature of N–N Bonding within High-Pressure Noble-Metal Pernitrides and the Prediction of Lanthanum Pernitride. *J. Am. Chem. Soc.* **2010**, *132*, 2421–2429.

(21) Yu, S.; Zeng, Q.; Oganov, A. R.; Frapper, G.; Zhang, L. Phase stability, chemical bonding and mechanical properties of titanium nitrides: a first-principles study. *Phys. Chem. Chem. Phys.* **2015**, *17*, 11763–11769.

(22) Kohn, W.; Sham, L. J. Self-Consistent Equations Including Exchange and Correlation Effects. *Phys. Rev.* **1965**, *140*, A1133–A1138.

(23) Hohenberg, P.; Kohn, W. Inhomogeneous Electron Gas. *Phys. Rev.* **1964**, *136*, B864–B871.

(24) Kulkarni, A.; Schön, J. C.; Doll, K.; Jansen, M. Structure Prediction of Binary Pernitride MN_2 Compounds ($M = Ca, Sr, Ba, La,$ and Ti). *Chem. - Asian J.* **2013**, *8*, 743–754.

(25) Zerr, A.; Miehe, G.; Riedel, R. Synthesis of cubic zirconium and hafnium nitride having Th_3P_4 structure. *Nat. Mater.* **2003**, *2*, 185–189.

(26) Eremets, M. I.; Gavriluk, A. G.; Serebryanaya, N. R.; Trojan, I. A.; Dzivenko, D. A.; Boehler, R.; Mao, H. K.; Hemley, R. J. Structural transformation of molecular nitrogen to a single-bonded atomic state at high pressures. *J. Chem. Phys.* **2004**, *121*, 11296–11300.

(27) Gregoryanz, E.; Goncharov, A. F.; Hemley, R. J.; Mao, H.-k.; Somayazulu, M.; Shen, G. Raman, infrared, and x-ray evidence for new phases of nitrogen at high pressures and temperatures. *Phys. Rev. B: Condens. Matter Mater. Phys.* **2002**, *66*, 224108.

(28) Yakovenko, E. V.; Aleksandrov, I. V.; Goncharov, A. F.; Stishov, S. M. Cubic boron nitride at high pressures: equation of state and Raman light scattering. *Sov. Phys. JETP* **1989**, *68*, 1213–1215.

(29) Angel, R. J. Equation of State. In *High Temperature High Pressure Crystal Chemistry*; Hazen, R. M., Downs, R. T., Eds.; Mineralogical Society of America: 2000; Vol. 41.

(30) Perdew, J. P.; Burke, K.; Ernzerhof, M. Generalized Gradient Approximation Made Simple. *Phys. Rev. Lett.* **1996**, *77*, 3865–3868.

(31) Perdew, J. P.; Chevary, J. A.; Vosko, S. H.; Jackson, K. A.; Pederson, M. R.; Singh, D. J.; Fiolhais, C. Atoms, molecules, solids, and surfaces: Applications of the generalized gradient approximation for exchange and correlation. *Phys. Rev. B: Condens. Matter Mater. Phys.* **1992**, *46*, 6671–6687.

(32) Perdew, J. P.; Ruzsinszky, A.; Csonka, G. I.; Vydrov, O. A.; Scuseria, G. E.; Constantin, L. A.; Zhou, X.; Burke, K. Restoring the Density-Gradient Expansion for Exchange in Solids and Surfaces. *Phys. Rev. Lett.* **2008**, *100*, 136406.

(33) Gou, H.; Hou, L.; Zhang, J.; Sun, G.; Gao, L.; Gao, F. Theoretical hardness of PtN_2 with pyrite structure. *Appl. Phys. Lett.* **2006**, *89*, 141910.

(34) Kawada, I.; Kato, K.; Yamaoka, S. Strontium disulphide prepared at high pressure. *Acta Crystallogr., Sect. B: Struct. Crystallogr. Cryst. Chem.* **1976**, *32*, 3110–3111.

(35) Jiang, C.; Lin, Z.; Zhao, Y. Thermodynamic and Mechanical Stabilities of Tantalum Nitride. *Phys. Rev. Lett.* **2009**, *103*, 185501.

(36) Maintz, S.; Deringer, V. L.; Tchougréeff, A. L.; Dronskowski, R. Analytic projection from plane-wave and PAW wavefunctions and application to chemical-bonding analysis in solids. *J. Comput. Chem.* **2013**, *34*, 2557–2567.

(37) Deringer, V. L.; Tchougréeff, A. L.; Dronskowski, R. Crystal Orbital Hamilton Population (COHP) Analysis As Projected from Plane-Wave Basis Sets. *J. Phys. Chem. A* **2011**, *115*, 5461–5466.

(38) Dronskowski, R.; Bloechl, P. E. Crystal orbital Hamilton populations (COHP): energy-resolved visualization of chemical bonding in solids based on density-functional calculations. *J. Phys. Chem.* **1993**, *97*, 8617–8624.

(39) Bader, R. F. W. *Atoms and Molecules*; Oxford University Press: 1994; p 458.

(40) Zhang, R. F.; Legut, D.; Fu, Z. H.; Veprek, S.; Zhang, Q. F.; Mao, H. K. Mechanical strength and electronic instabilities in ultra-incompressible platinum dinitrides. *Phys. Rev. B: Condens. Matter Mater. Phys.* **2015**, *92*, 104107.